Sunday O. Olatunji and Taoreed O. Owolabi*

Modeling the band gap of spinel nano-ferrite material using a genetic algorithm based support vector regression computational method

https://doi.org/10.1515/ijmr-2022-0058 Received February 8, 2022; accepted October 4, 2022; published online February 7, 2023

Abstract: Spinel nano-ferrite compounds have attracted significant interest in industrial, scientific and technological communities as a result of their promising and unique features especially at nano-scale range. The present and future potentials of spinel nano-ferrite materials cut across several applications such as biotechnology, magnetic storage, sensors, magnetic hyperthermia, microwave absorbance and photo-catalysis. Enhancing the photocatalytic application of spinel nano-ferrite materials involves accommodation of foreign materials into the parent compound as well as appropriate fabrication technique which respectively alter the crystal structure and nano-size of the spinel nanoferrite materials. This work implements the crystal lattice distortion and the size of nano-particles to develop, for the first time, hybridization of a support vector regression algorithm with a genetic algorithm for estimating the energy gap of doped spinel nano-ferrite materials. The developed hybrid genetic algorithm based support vector regression model was built using two hundred different spinel nano-ferrite materials doped with varieties of materials and synthesized through various methods. The developed genetic algorithm based support vector regression model that is characterized by low root mean square error and mean squared error of 0.3075 eV and 0.095 eV respectively, was further validated using eighteen different spinel nano-ferrite materials and the estimated energy gaps agree excellently with the experimental values. The influence of magnesium, aluminum and lanthanum on the band gap of spinel ferrite nanoparticles was investigated and studied using the developed genetic algorithm based

Sunday O. Olatunji, College of Computer Science and Information Technology, Imam Abdulrahman Bin Faisal University, Dammam, Saudi Arabia, E-mail: osunday@iau.edu.sa

support vector regression model. The developed model in this work ultimately provides a quick, accurate and precise method of characterizing the band gap of spinel nanoferrite materials while circumventing experimental stress with conservation of appreciable time and other valuable resources.

Keywords: Energy band gap; Genetic algorithm; Lattice parameter; Nano-size; Spinel nano-ferrite materials; Support vector regression.

1 Introduction

Spinel ferrite nano-particles are technologically important materials with versatile applications in magnetic drug delivery, magnetic recording, energy storage, sensor fabrication, heterogeneous catalysis, waste water treatment, and photo-Fenton processes among others [1-3]. The spinel ferrite magnetic characteristic contributes immensely to the recycling feature of the material with retention of its known catalytic activity. Both tetrahedral and octahedral voids in spinel ferrite nano-particles are occupied by metal ions while the presence of oxygen atoms results in cubic close packing. Although transition metal ions have site preference which has been studied extensively elsewhere, metal ion distribution significantly influences the electrical, magnetic, structural, and optical properties of spinel ferrite nano-particles [3]. Altering the spinel ferrite nano-particle physical properties is achieved either by tuning the features of metal ions, changing the method of synthesis, sintering conditions or partial substitution of external particles referred to as dopants into structural lattice of spinel ferrite nano-particles [4]. The chemical methods of synthesis include combustion method, solid state reaction, co-precipitation route and microwave synthesis among others. The preparation conditions strongly influence the morphological and structural features of spinel ferrite nanoparticles such as size of the particles, surface state and chemical homogeneity while doping alters the cation distribution in tetrahedral as well as octahedral sites and thereby

^{*}Corresponding author: Taoreed O. Owolabi, Physics and Electronics Department, Adekunle Ajasin University, Akungba Akoko, Postal code 342111, Ondo State, Nigeria, E-mail: owolabitaoreedolakunle@gmail.com. https://orcid.org/0000-0002-6666-1755

changes the magnetic, electric, structural and optical characteristics.

Spinel ferrite nano-particles belong to a class of soft ferrite with general chemical formula AB_2O_4 and happen to be a type of nano-ferrite materials that principally combine mixed composition of metal ions and iron oxide. The oxygen anions of spinel ferrite nano-particles crystalize in faced center cubic structure while the metal cations A^{2+} and Fe³⁺ (B^{3+}) respectively occupy the tetrahedral and octahedral sites [4]. Although nano-ferrite materials can be grouped into hexagonal ferrites, garnet ferrites and spinel ferrites, spinel nano-ferrites are the most promising, explored and researched due to the stability of their lattice structure, easy tuning properties, simple crystal structure, ease of guest ion (dopant) accommodation, flexibility of cationic distribution and ease of chemical synthesis among others. Balancing of ions controls the cation allocation between the available intrinsic lattice sites and directly determines the properties of spinel ferrite nano-particles [2]. Accommodation of foreign materials, stoichiometric proportions of dopants, preparation and synthesis circumstances significantly influence the optical properties of spinel ferrite nano-particles. The nature and stoichiometry of the incorporated foreign materials alter the crystal lattice structure of spinel ferrite nano-particles while the preparation and synthesis circumstances influence the size of the spinel ferrite nano-particles. This research work employs the crystal lattice parameter of the doped spinel ferrite nano-particles and the nano-size of the material to estimate the band gap energy of spinel ferrite nano-particles using support vector regression coupled with genetic algorithm for parameter optimization.

Support vector regression (SVR) belongs to the class of intelligent algorithms with statistical learning theory formulation [5]. The algorithm aims at minimizing the generalized error bound using the principle of structural risk minimization and thereby results in excellent prediction and generalization capacity. Since SVR transforms and maps data to high dimensional feature space, the adopted kernel trick and function conveniently circumvent the problem associated with the curse of dimensionality whereby the variable dimension in real space becomes inconsequential to the inner product performed in feature space of high dimension [6]. These important features of the SVR algorithm have resulted in wide applicability of the algorithm in diverse fields of study and disciplines including materials science, laser spectroscopy and superconductivity among others [7–9]. The user defined parameters of the SVR algorithm need to be properly tuned for precision and

accuracy enhancement using a heuristic algorithm. The choice of genetic algorithm (GA) for parameter optimization in this work is due to the intrinsic features of genetic algorithm such as avoidance of local convergence, quick convergence, low possibility of premature convergence as well as the ease of its implementation.

The arrangement of the rest of the manuscript is as follows: Section 2 discusses the mathematical formulation of both genetic algorithm and support vector regression. Presentation the computational methodology and the acquisition details of the employed dataset as extracted from more than two hundred doped spinel nano-ferrite materials is depicted in Section 3 of the manuscript. Section 4 discusses the research outcomes with the results of the optimization method and factors influencing the convergence of the algorithm. Comparison of the measured energy gap with the estimated values using the GA-SVR developed model is also presented in Section 4 of the manuscript. Section 5 summarizes the manuscript.

2 Mathematical formulation and background of the developed hybrid model

This section presents the background of the support vector regression intelligent algorithm employed. The operation details and principles of genetic algorithm are also present.

2.1 Support vector regression

A support vector regression algorithm aims at acquiring pattern linking the descriptors μ with the desired target $B_g(\mu)$ through training of dataset samples S = $\left\{\left(\mu_1, B_g^*\right), \ldots, \left(\mu_n, B_{gn}^*\right)\right\}, B_{gn}^* \in \mathbb{R}$ (where B_g^* represents the measured band gap) by approximating the function to a form presented in Equation (1) [9].

$$B_{\sigma}(\mu) = \omega^T \mathbf{x} + d \tag{1}$$

where μ stands for the predictors that include the lattice parameter and the size of spinel ferrite nano-particles while $B_{\sigma}(\mu)$ stand for the estimated energy gap. The goal of the algorithm is to ensure that the difference between $B_{\sigma}(\mu)$ and the measured band gap B_g^* is very small while only slight deviation of ε is tolerated. Thus, ω and d model parameters are to be determined through convex optimization which aims at minimizing Equation (2) with inclusion of ε – insensitive loss ρ presented in Equation (3) [7].

Minimize
$$\frac{1}{\omega} \|\omega\|^2 + C \sum_{j=1}^m \rho \left(B_{\mathbf{g}}(\mu_j) - B_{\mathbf{g}j}^* \right)$$
 (2)

$$\rho(q) = \begin{cases} 0 & \text{if } |q| \le \varepsilon \\ |q| - \varepsilon & \text{otherwise} \end{cases}$$
 (3)

where C is the penalty factor (also known as the regularization factor).

Inclusion of positive non-zero variables called slack variables (γ and γ^*) modifies Equations (2) to (4) with constraints presented in Equation (5) [10].

Minimize
$$\frac{1}{\omega}$$
, $\frac{1}{2} \|\omega\|^2 + C \sum_{i=1}^{m} (\chi + \chi^*)$ (4)

$$B_{g}(\mu_{j}) - B_{gj}^{*} \le \varepsilon + \chi_{j}$$

$$B_{gj}^{*} - B_{g}(\mu_{j}) \le \varepsilon + \chi_{j}^{*}$$

$$\chi_{j}^{*} \ge 0, \ \chi_{j} \ge 0, \ j = 1, 2, 3, \dots, m$$
(5)

Introduction of Lagrange multipliers (ψ, ψ^*) conveniently transforms the problem to quadratic optimization presented in Equation (6) with the conditions depicted in Equation (7)

Maximize
$$\psi, \psi^* \sum_{j=1}^m B_{gj}^* \left(\psi_j^* - \psi_j \right) - \varepsilon \left(\psi_j^* + \psi_j \right)$$
$$- \frac{1}{2} \sum_{i=1}^m \sum_{j=1}^m \left(\psi_j^* - \psi_j \right) \left(\psi_i^* - \psi_i \right) \mathbf{x}_j^T \mathbf{x}_i$$
(6)

subjected to
$$\sum_{j=1}^{m} (\psi_j^* - \psi_j) = 0$$
$$0 \le \psi_j, \ \psi_i^* \le C$$
 (7)

The solution of the quadratic optimization yields ψ_i with the condition that $0 \le \psi_i \le C$. After mapping the lattice parameters and the size of spinel ferrite nano-particles, the bias d and other model parameter ω are determined and presented in Equations (8) and (9), respectively where $\theta(\mu)$ represents the eigenvector.

$$d = B_{gj}^* + \varepsilon - \sum_{j=1}^m \left(\psi_j^* - \psi_j \right) \theta(\mathbf{\mu}_j)^T \theta(\mathbf{\mu}_j)$$
 (8)

$$\omega = \sum_{i=1}^{m} \left(\psi_j^* - \psi_j \right) \theta(\mathbf{\mu_j}) \tag{9}$$

Equation (9) substitution in Equation (1) leads to Equation (10)

$$B_{g}(\mu) = \sum_{j=1}^{m} \left(\psi_{j}^{*} - \psi_{j} \right) \vartheta(\mu, \mu_{j})$$
 (10)

where $\theta(\mu, \mu_i) = \theta(\mu_i)^T \theta(\mu_i)$ represents the kernel function for data mapping.

The formulation for the employed Gaussian function is shown in Equation (11) [6].

$$\vartheta(\boldsymbol{\mu}, \boldsymbol{\mu}_{j}) = \exp\left\{-\lambda \left\|\boldsymbol{\mu} - \boldsymbol{\mu}_{j}\right\|^{2}\right\}$$
 (11)

where λ represents the kernel parameter.

2.2 Genetic algorithm

A genetic algorithm is a population based random search optimization algorithm that shares operational principle resemblance with the biological evolution genetic mechanism proposed by Darwin [11]. It adaptively controls the process of global searching purposely to attain global convergence through a parallel, efficient and global search method that automatically records and acquires the knowledge of probable possible solutions within the search space. The feasible and probable solutions representing the hyperparameters of an SVR algorithm are expressed as individuals called chromosomes within genetic algorithm operational principles. The element contained in the chromosome called a gene is a true representation of a single solution to be optimized while three hyper-parameters such as the regularization parameter, epsilon and kernel parameter, are contained in a single solution referred to as a gene while all the possible values in the gene are called the alleles. Specifically, a combination of hyper-parameters represent a single solution called a chromosome while the regularization parameter, epsilon and kernel parameter are individually called the gene and their specific values are called the alleles [7]. The operations involved in genetic algorithm implementation include selection, crossover and mutation. A selection operator is employed within the genetic algorithm operational principle with a specific probability for transition from one generation to another through reproduction and population replacement. The fitness of an individual in a population has a strong reflection on the possibility of being retained and selected for inclusion in the subsequent generation. Individuals with good characters are selected and retained in this contribution through a stochastic universal selection procedure [12]. Crossover operation involves random selection of two parents within the population followed by gene exchange and recombination, resulting in a new individual with inherited features from their parents. The mutation operation leads to varieties of trait within the population and prevents being trapped within a local solution.

3 Data acquisition and computational hybridization methodology

The sources of employed dataset and their descriptions are presented in this section. A computational method of hybridizing support vector regression and genetic algorithm is also presented.

3.1 Description of lattice distortion and the size of nano-particles for spinel nano-ferrite materials employed in model development

The predictors to the developed GA-SVR model include crystal lattice parameter and the size of spinel nano-ferrite. The descriptors and the corresponding energy band gaps are extracted from the literature [2, 13-59]. The employed dataset consists of spinel ferrite nano-particles doped with different foreign materials. Incorporation of foreign materials into the parent spinel nano-ferrite alters and distorts the lattice parameter of the material depending on the ionic radius of the dopant and the substituted ions. In order to assess the potentials of the proposed model for precise estimation of the energy gap, statistical analysis was conducted on the employed set of data and the outcomes of the analysis are shown in Table 1. The table shows values of the mean (average value) through which the overall content of the dataset can be inferred since the sum of deviations of each value from the average value is always zero. Standard deviations that measure the consistency in the dataset as extracted from measurement to measurement are also presented. The maximum and minimum values presented are insightful for understanding the range and boundaries of the dataset. The presented coefficients of correlation give the extent and degree of linear relationship existing between the target and predictors. The cross-plot correlation between the size of nano-particles, the crystal lattice parameter and experimental band gap is presented

in Figure 1. The figure shows spatial distribution of all the employed data-points in three dimensions. The distribution presented in Figure 1 shows the inability of a unique linear function to relate the descriptors with the energy gaps. Therefore, this research work aims at developing a single and universal relation through which the energy band gap of any spinel nano-ferrite based compounds can be estimated and determined. Hence, we have developed a GA-SVR model for this purpose.

3.2 Computation hybridization of support vector regression and genetic algorithms

Genetic algorithm hybridization with support vector regression algorithms as well as other computational tasks were conducted using the MATLAB computing facility. The developed GA-SVR model estimates the energy band gap of doped spinel ferrite nano-particles using the size of the particle and the crystal lattice parameter as inputs to the model. Data-points from two hundred spinel ferrite nano-materials available for simulation were separated into training and testing in the ratio of 8:2 where one hundred and sixty datapoints were allotted for model training and forty data-points were assigned for model testing and hyper-parameter setting using the genetic algorithm. Data-points were randomized to ensure that the investigated samples are well and evenly distributed so that model testing fell within what the model learnt previously. The developed model was further validated using eighteen doped samples of spinel ferrite nano-materials that were excluded from the training and testing phase of model development. The hyper-parameters optimized by genetic algorithms were the epsilon, kernel parameter of the best fit kernel function for data transformation and regularization factor. The details of the computational procedures are itemized as follows:

Step I: Population initialization: this stage of computational method initializes and generates a population of probable solutions within a defined search space. The search space of the hyper-parameter regularization factor extends between 1 and 500 while that of the epsilon and

Table 1: The results of each of the statistical parameters for the employed descriptors and energy band gap.

Statistical parameter	Lattice parameter a (Å)	Size of nano-particles <i>D</i> (nm)	Energy band gap (eV)
Mean	8.392	24.806	2.212
Standard deviation	0.079	14.691	0.758
Maximum	8.726	71.000	5.000
Correlation coefficient	0.1922	-0.0441	-
Minimum	8.223	1.800	1.300

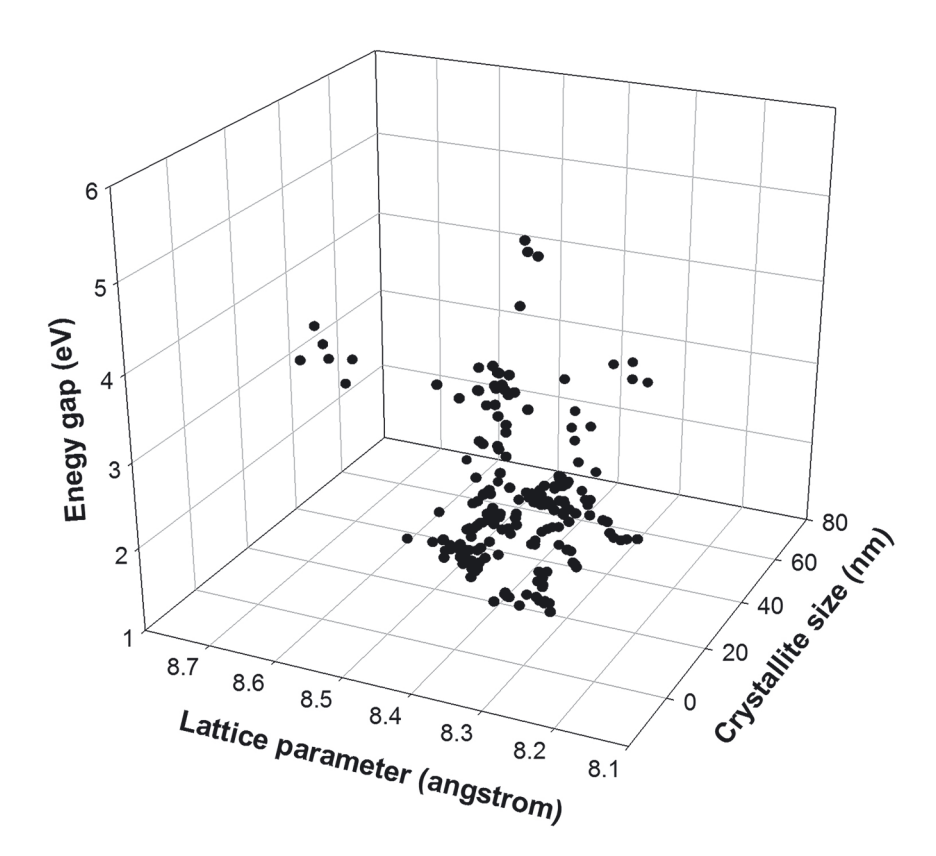


Figure 1: Correlation cross-plot in three dimensions.

kernel parameter range from 0.1 to 0.001. Variations of number of population were investigated purposely to determine the contribution of the number of initial population to the precision and convergence of the model.

Step II: Fitness computation for chromosome evaluation: Evaluation of each of the chromosomes in the population was carried out using root mean square error as a measure of fitness were a low value corresponds to more fit chromosome and high value corresponds to less fit chromosome. While computing the fitness, the SVR algorithm is incorporated and hybridized with the genetic algorithm as detailed below:

- Selection of the kernel function from polynomial, sigma and Gaussian function for data mapping and transformation to the feature space.
- Selection of a chromosome that represents the regularization factor, kernel parameter and epsilon within the population.
- Training of the SVR algorithm using (i) the selected chromosome in $\mathbf{Step}\ \mathbf{b}$, (ii) the selected kernel function in Step a, and (iii) the training set of data.
- Evaluation of the performance of trained SVR algorithm in **Step c** using root mean square error.

- Repeat Step b to Step d for all the chromosomes in the population and rank the best chromosome on the basis of root mean square error using the principle that the lower the better.
- Further evaluation of the trained SVR algorithm using the testing set of data and record the values of the root mean square error.
- Repeat **Step b** to **Step f** for the other activation function and save the details of the model with lowest root mean square error. The saved model details include the support vectors, regularization factor, performance measuring parameters for training and testing set of data, epsilon and kernel parameters.

Step III: Algorithm reproduction stage: In order to replace the population with chromosomes of better quality, a selection operation was carried out using probability selection of 0.8. This chosen value of probability gives better a chance to chromosome with better fitness to proceed to the next generation.

Step IV: Implementation of crossover operator: Exchange of subsequences and portions for offsprings selection was carried out through a crossover operation. 0.65 probability of crossover was maintained in order to replace the weaker individual from the subsequent population.

Step V: Randomness of string positions through mutation operation: Probability of 0.009 was implemented for mutation and altering of randomness of position of strings.

Step VI: *Stopping conditions*: The algorithm is brought to a stop when the same value of root mean square error is obtained for forty consecutive generations.

Step VII: The final GA-SVR model is developed through implementation of hyper-parameters generated from GA.

4 Results and discussion

The results of the hybrid GA-SVR are discussed in this section. The convergence of the genetic optimization algorithm and hyper-parameters is also presented as the number of initial population changes. Comparison of the estimates of GA-SVR with the measured energy gap for diverse kinds of spinel ferrite nano-particles is contained in this section.

4.1 Convergence of hyper-parameters as initial population number changes

The significance of varying the population size exploiting and exploring the search space of the hybrid GA-SVR model on model convergence is depicted in Figure 2. When 200 chromosomes are in the search space, the algorithm

converges to a local solution as presented in Figure 2. The global convergence is attained with a population of 50 exploring the search space, as shown in the figure. Increasing the population from 50 to 100 throws the model back into local solution as depicted in Figure 2. This can be attributed to weak exploitation capacity of the model consequent upon the presence of a large number of chromosomes exploiting a limited search space. The convergence of regularization/penalty factor with the chromosome population is shown in Figure 3. While varying the size of the population, the penalty factors (that trades-off model complexity and the allowed error threshold) begin the convergence at the same point of iteration. This is a clear indication of the robustness of the developed hybrid model. Convergence of the maximum allowed error threshold called epsilon as the chromosome population is changing is presented in Figure 4. Increase in population size gradually shifts the convergence values of epsilon towards large values as depicted in the figure. Since epsilon measures the maximum allowed error and the lower value is attributed to a good model, the optimum population size exploiting and exploring the space as can be deduced from the figures is fifty. Similar convergence for the kernel parameter is presented in Figure 5. The kernel parameter controls the transformation and mapping of data to the feature space for regression function construction. Change in the number of chromosomes to higher values shifts the value of the Gaussian function kernel parameter to a lower value. The hyper-parameters that optimize the developed SVR model are contained in Table 2.

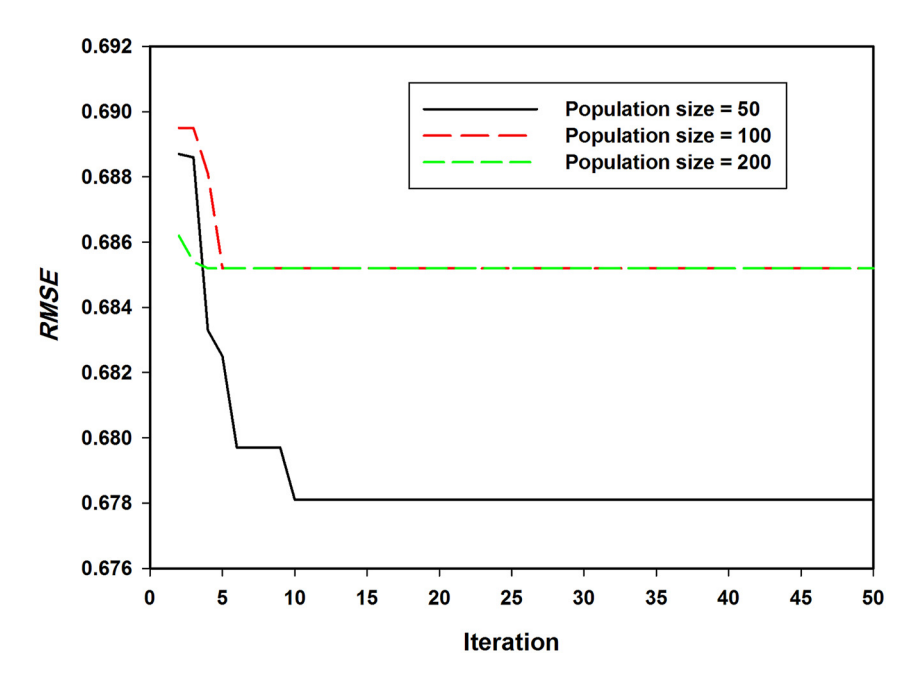


Figure 2: Convergence of GA-SVR model at different population sizes.

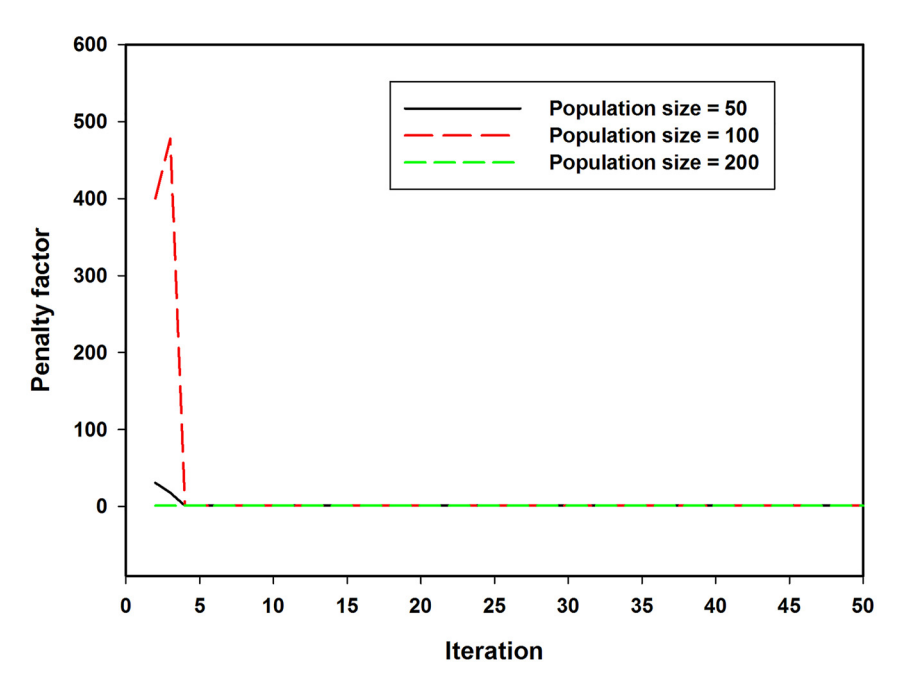


Figure 3: Convergence of penalty factor at various population sizes.

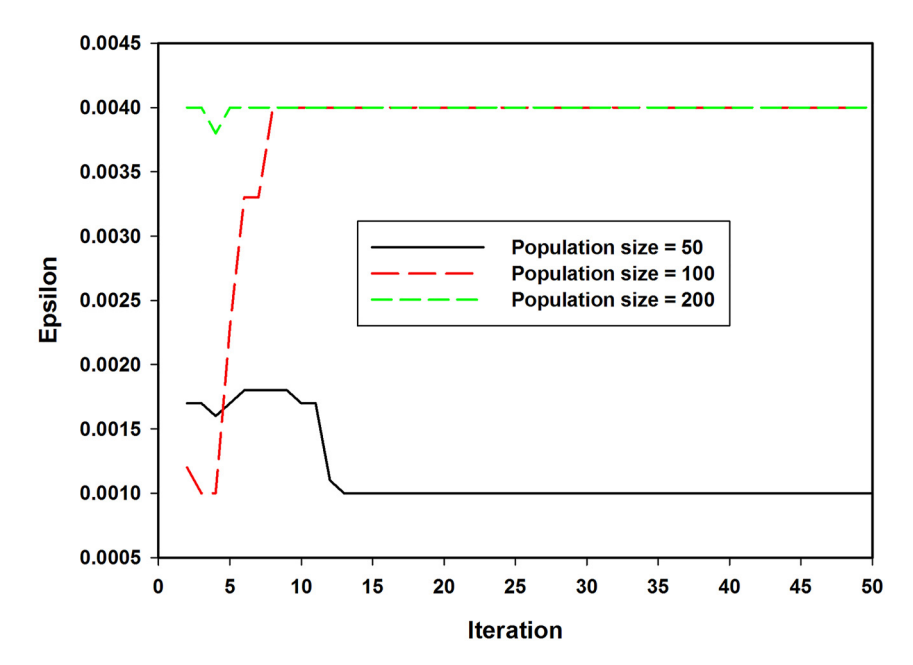


Figure 4: Convergence of epsilon at various population sizes.

4.2 Evaluation of model performance through error metrics

Evaluation of the hybrid model was conducted during the training, testing and external validation stage of model development using mean squared error (MSE), correlation coefficient (CC) and root mean square error (RMSE). The training phase acquires support vectors which are

optimized through parameter tuning with the testing dataset using the genetic algorithm. During the validation stage, the developed model only used its saved support vectors for estimation and the model is only supplied with the lattice parameter of doped spinel ferrite nano-particles and the size of the nano-particles. During parameters tuning using the testing set of data, the recorded RMSE and

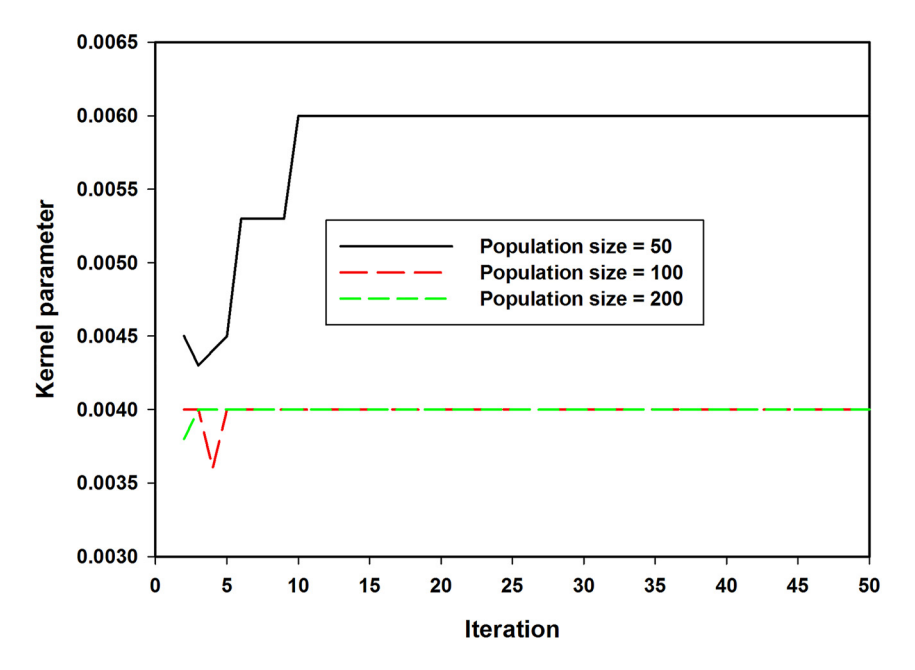


Figure 5: Convergence of kernel parameter at various population sizes.

Table 2: Best hyper-parameters obtained from GA.

Hyper-parameter	Best value
Hyper-parameter lambda	E-7
Population number	50
Kernel parameter	0.0045
Kernel function	Gaussian
Penalty factor (C)	30.682
Epsilon	0.0017

MSE for the developed model are 0.6781 eV and 0.45984 eV, respectively. Figure 6 presents the comparison of the GA-SVR model during training and external validation stages. The developed GA-SVR performs better during validation stage than training phase with performance improvement

of 89.16%, 98.83% and 2.72% using *RMSE*, *MSE* and *CC*, respectively.

It is worth mentioning that the validation stage involved feeding the GA-SVR model with only the descriptors (lattice parameter and size of the nano-particles) while the GA-SVR employs the saved support vectors for its estimation. The values of the parameters that assess the performance of the GA-SVR model are presented in Table 3 for both training and validation stages.

The performance improvement observed in the validation dataset over that of the training set can be attributed to the implementation of a regularization term (represented as C in Equation (2)) during the training phase of model development and thereby inflating the training loss. The loss function while validating the model comprises only the prediction error without the regularization term, which generally results into lower error than the training set.

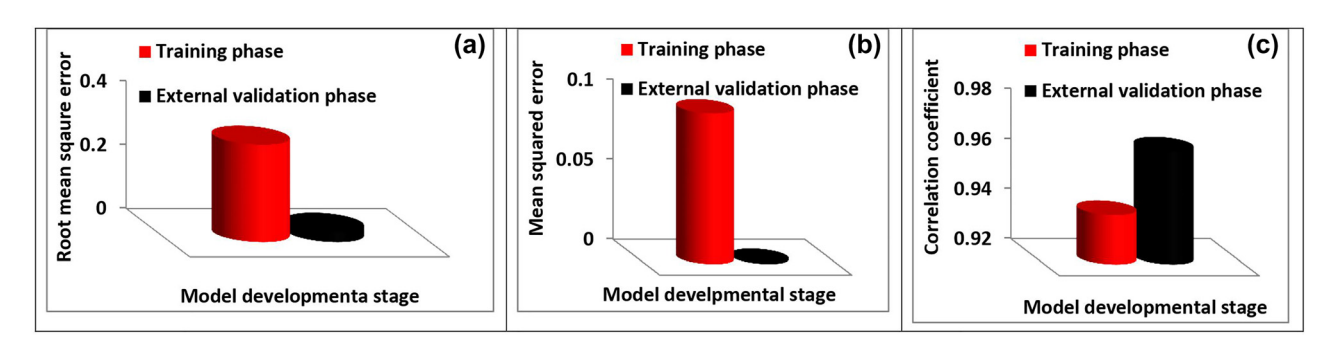


Figure 6: Model evaluation parameters and their comparisons at different developmental stages on the basis (a) RMSE (b) MSE (c) CC.

Table 3: Evaluation parameters and their corresponding values.

Dataset	сс	RMSE	MSE
Training	0.9399	0.3075	0.0945
External validation	0.9654	0.0333	0.0011

Only support vectors saved during the training phase of model development were implemented during validation stage.

4.3 Band gap tailoring effect of magnesium incorporation on cobalt ferrite spinel nanoparticle using the developed **GA-SVR** model

The results of the influence of magnesium particles incorporated into the crystal structure of cobalt ferrite spinel nanoparticles on the band gap are shown in Figure 7. The outcomes of the GA-SVR model agree excellently with the experimental values of energy gap [57]. Magnesium incorporation into the parent ferrite spinel lowers the lattice parameter of the parent compound due to the lower ionic radius of magnesium as compared to cobalt, while increase in the concentration of magnesium dopants results in lattice distortion without altering the lattice symmetry. The observed reduction in crystallite size also connects with the variation in the ionic radii of the dopants and substituted element [57]. The stretching vibration in tetrahedral sites of $Fe^{3+} - O^{2-}$ is responsible for the observed effect of dopants presented in Figure 7. Level formation energy of sub-band consequent upon the existence of interfacial defects caused by dopants is also responsible for the observed band gap adjustment. The developed model well captures the experimental trend of band gap variation in these ferrite nano-particles.

4.4 Energy gap effect of aluminium dopants on nickel ferrite spinel material using the developed hybrid GA-SVR model

The significance of aluminum incorporation in nickel ferrite spinel nano-particles on the band gap, as obtained using the developed GA-SVR model is presented in Figure 8. The experimentally measured band gap is also presented in the figure for comparison [58]. The occupancy of aluminum ion dopants in the lattice structure of the host nickel ferrite is manifested from the observed contraction in lattice parameter as well as lattice strains. When lattice strains occur, internal stress is built up and this prevents further growth of particle size which results in reduction in nanoparticle size. The observed change in band gap with increase in the concentration of aluminum is connected with the nature of the aluminum dopants while the predicted band gaps using the developed GA-SVR model agree excellently with the measured values.

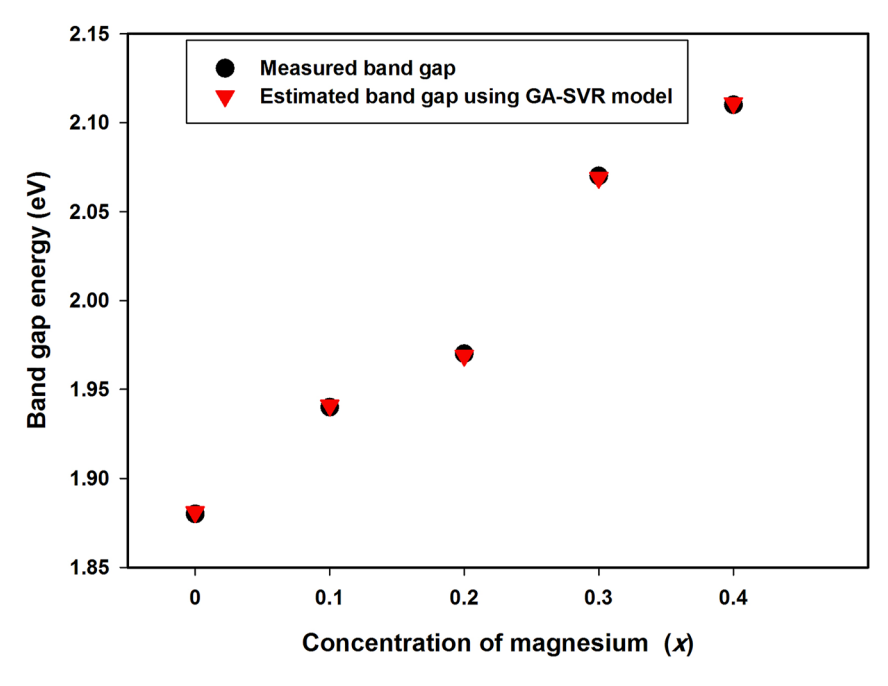


Figure 7: Influence of magnesium dopants on the band gap of cobalt ferrite spinel nanoparticle.

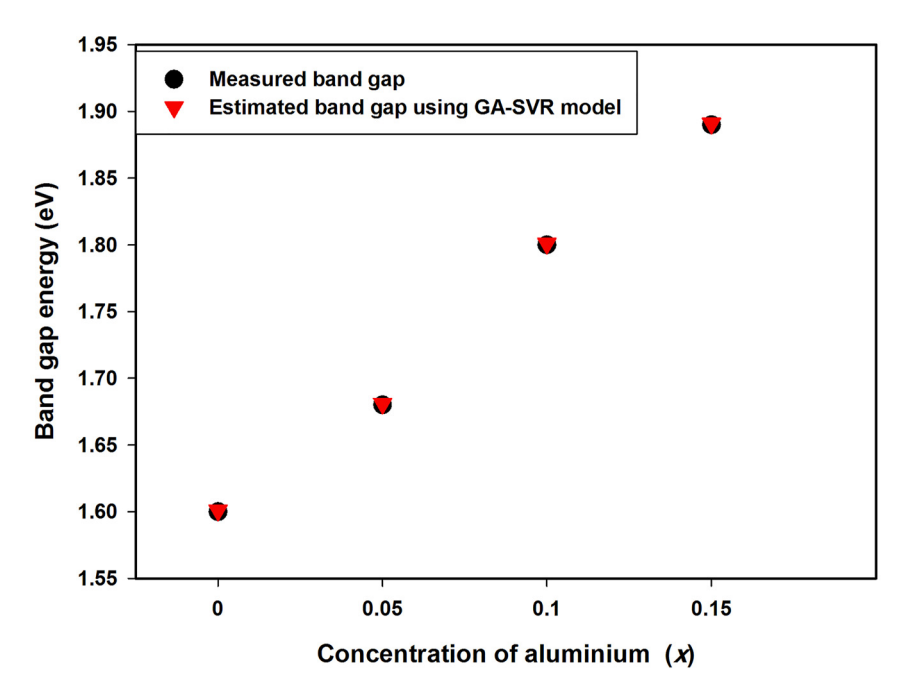


Figure 8: Effect of aluminum dopants on the band gap of nickel ferrite spinel material.

4.5 Significance of lanthanum in band gap tuning of ferrite spinel material using the developed GA-SVR model

The band gap adjustment potential of lanthanum is presented in Figure 9 using the developed GA-SVR model and experimental measurement for comparison [13]. The results

of the developed GA-SVR agree perfectly well with the measured values. A steadily observed lattice parameter variation is attributed to initial formation of impurities at the grain boundaries of the host spinel ferrite followed by subsequent diffusion of the dopants with the substituted element. The observed alteration in band gap energy is due to

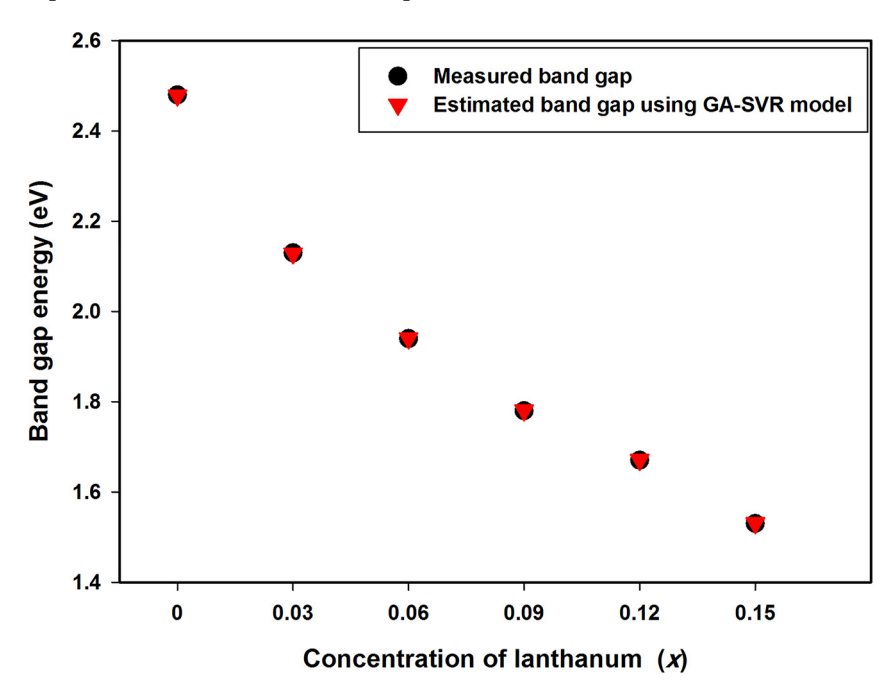


Figure 9: Band gap influence of lanthanum dopants on ferrite spinel material.

Table 4: Comparison of the estimated band gaps during external validation with the measured values.

Spinel ferrite compound	Measured band gap energy (eV)	Estimated band gap energy using GA-SVR (eV)	% error
NixFe _{3-x} O ₄ ($x = 0.75$)	2.52 [48]	2.519	0.039
$NixFe_{3-x}O_4$ (x = 1.0)	2.53 [48]	2.529	0.040
$NixFe_{3-x}O_4$ (x = 1.5)	2.56 [48]	2.559	0.039
$Ni_{1-x}Zn_xFe2O_4 (x = 0)$	2.60 [47]	2.115	18.642
$Ni_{1-x}Zn_xFe_2O_4$ (x = 0.1)	2.41 [47]	2.409	0.041
$Ni_{1-x}Zn_xFe_2O_4$ (x = 0.3)	2.26 [47]	2.259	0.044
$Ni_{1-x}Zn_xFe_2O_4$ (x = 0.5)	2.14 [47]	2.115	1.154
$Ni_{1-x}Zn_xFe2O_4$ (x = 0.7)	2.06 [47]	2.061	0.0485
$Ni_{1-x}Zn_xFe_2O_4$ (x = 1)	1.93 [47]	1.931	0.052
$Ni_{1-x}Cd_xFe_2O_4 (x = 0)$	2.11 [44]	2.111	0.047
$Ni_{1-x}Cd_xFe_2O_4$ (x = 0.2)	2.04 [44]	2.115	3.691
$Ni_{1-x}Cd_xFe_2O_4$ (x = 0.4)	1.99 [44]	1.991	0.050
$Ni_{1-x}Cd_xFe_2O_4$ (x = 0.6)	1.96 [44]	1.961	0.051
$Ni_{1-x}Cd_xFe_2O_4$ (x = 0.8)	1.90 [44]	1.901	0.053
$MnLa_x Fe_{2-x} O_4 (x = 0)$	1.25 [33]	1.251	0.080
$MnLa_x Fe_{2-x} O_4 (x = 0.04)$	1.30 [33]	1.301	0.076
$MnLa_x Fe_{2-x} O_4 (x = 0.06)$	1.34 [33]	1.341	0.074
$MnLa_x Fe_{2-x} O_4 (x = 0.08)$	1.38 [33]	1.381	0.072
		Mean absolute percentage error (MAPE)	1.350

some Fe³⁺ movement from tetrahedral sites to octahedral sites.

4.6 External validation of the developed **GA-SVR** model

In order to further justify the precision and accuracy of the developed GA-SVR model, the model was further validated with eighteen different spinel ferrite nanoparticles that were not included in the training and testing phase of model development. In this implementation, the developed hybrid model was only fed with the lattice parameter after dopant incorporation and the size of nanoparticles while the model estimates the corresponding band gap through support vectors saved during the training stage of model development. Table 4 presents the comparison of the model estimates and the measured band gap for the investigated compounds. The sources of data for each of the compounds are included in the table. The mean absolute percentage error (MAPE) of 1.35 eV was recorded during external validation which further confirms excellent generalization capacity of the developed model in real life practical scenarios.

5 Conclusions

A hybrid model for estimating the band gap of spinel ferrite nanoparticles was developed using a genetic algorithm and support vector regression intelligent model. The developed GA-SVR employed the distorted lattice parameter and the size of nanoparticles extracted from two hundred spinel ferrite nanoparticles doped with varieties of foreign materials for pattern acquisition. The developed hybrid model was evaluated using RMSE, CC and MSE. The developed model investigated the influence of magnesium, aluminum and lanthanum on band gaps of some doped spinel ferrite nanoparticles and the obtained band gap using the model agreed excellently with the measured values. The hybrid GA-SVR model also estimated the band gap of eighteen spinel ferrite nanoparticles with different dopants nature and concentration during external validation and the obtained results agreed well with measured values. The precision demonstrated by the developed GA-SVR model will facilitate quick determination of the band gap of spinel ferrite nanoparticles and the influence of any dopants on the band gap of spinel ferrite can be determined for band gap enhancement in photocatalysis.

Author contributions: All the authors have accepted responsibility for the entire content of this submitted manuscript and approved submission.

Research funding: None declared.

Conflict of interest statement: Authors declare no Competing Financial or Non-Financial Interests.

Data availability statement: The raw data required to reproduce these findings are available in the references cited in Section 3.1 of the manuscript.

References

- 1. Almessierea M. A., Slimania Y., Gunerc S., Sertkold M., Korkmaze A. D., Shirsath S. E., Baykal A. Sonochemical synthesis and physical properties of Co_{0.3}Ni_{0.5}Mn_{0.2}Eu_xFe_{2-x}O₄ nano-spinel ferrites. *Ultrason. Sonochem.* 2019, *58*, 104654. https://doi.org/10.1016/j .ultsonch.2019.104654.
- 2. Slimani Y., Unal B., Almessiere M. A., Korkmaz A. D., Shirsath S. E., Yasin G., Trukhanov A. V., Baykal A. Investigation of structural and physical properties of Eu³⁺ ions substituted Ni_{0.4}Cu_{0.2}Zn_{0.4}Fe₂O₄ spinel ferrite nanoparticles prepared via sonochemical approach. Results Phys. 2020, 17, 103061. https://doi.org/10.1016/j.rinp.2020
- 3. Almessiere M. A., Slimani Y., Korkmaz A. D., Guner S., Sertkol M., Shirsath S. E., Baykal A. Structural, optical and magnetic properties of Tm3+ substituted cobalt spinel ferrites synthesized via sonochemical approach. *Ultrason. Sonochem.* 2019, 54, 1–10. https://doi.org/10.1016/i.ultsonch.2019.02.022.
- 4. Zhang J., Bai H., He S., Ma Y., Jiang B., Liu P., Yuan H. Effects of structure and electronic properties of spinel ferrites on their emissivity in middle and short wavebands. J. Solid State Chem. 2020, 282, 121089. https://doi.org/10.1016/j.jssc.2019.121089.2019.
- 5. Vapnik V. *The Nature of Statistical Learning Theory*; Springer: New-York Berlin Heidelberg, 1995.
- 6. Hu H., Yu J., Song Y., Chen F. The application of support vector regression and mesh deformation technique in the optimization of transonic compressor design. Aero. Sci. Technol. 2021, 112, 106589. https://doi.org/10.1016/j.ast.2021.106589.
- 7. Olatunji S. O., Owolabi T. O. Modeling superconducting transition temperature of doped MgB₂ superconductor from structural distortion and ambient temperature resistivity measurement using hybrid intelligent approach. Comput. Mater. Sci. 2021, 192, 110392. https://doi.org/10.1016/j.commatsci.2021.110392.
- 8. Shamsah S. M. I., Owolabi T. O. Modeling the maximum magnetic entropy change of doped manganite using a grid search-based extreme learning machine and hybrid gravitational search-based support vector regression. Crystals 2020, 10, 310. https://doi.org/10 .3390/cryst10040310.
- 9. Shamsah S. M. I., Owolabi T. O. Newtonian mechanics based hybrid machine learning method of characterizing energy band gap of doped zno semiconductor. Chin. J. Phys. 2020, 68, 493-506. https://doi.org/10.1016/j.cjph.2020.10.002.
- 10. Owolabi T. O., Akande K. O., Olatunji S. O. Estimation of surface energies of hexagonal close packed metals using computational intelligence technique. Appl. Soft Comput. 2015, 31, 360 – 368. https://doi.org/10.1016/j.asoc.2015.03.009.
- 11. Holland J. H. Genetic algorithms. Sci. Am. 1992, 267, 66 73. https:// doi.org/10.1038/scientificamerican0792-66.
- 12. Dufek A. S., Augusto D. A., Dias P. L. S., Barbosa H. J. C. Application of evolutionary computation on ensemble forecast of quantitative precipitation. Comput. Geosci. 2017, 106, 139-149. https://doi.org/ 10.1016/j.cageo.2017.06.011.
- 13. Cu N., Fe C., Aslam A., Morley N. A., Amin N., Imran M., Ajaz M., Ali A., Mahmood K., Bibi A., Iqbal F., Hussain S., Jamil Y. Study of structural, optical and electrical properties of La³⁺ doped ${\rm Mg_{0.25}Ni_{0.15}Cu_{0.25}Co_{0.35}Fe_{2-x}La_{x}O_{4}\ spinel\ ferrites.}\ \textit{Physica\ B:\ Phys.}$ Condens. Matter 2021, 602, 412565. https://doi.org/10.1016/j.physb .2020.412565.

- 14. Sadagat A., Almessiere M., Slimani Y., Guner S., Sertkol M., Albetran H., Baykal A., Shirsath S. E., Ozcelik B., Ercan I. Structural, optical and magnetic properties of Tb3+ substituted Co nanoferrites prepared via sonochemical approach. Ceram. Int. 2019, 45, 22538 - 22546. https://doi.org/10.1016/j.ceramint.2019.07
- 15. Almessiere M. A., Slimani Y., Kurtan U., Guner S., Sertkol M., Shirsath S. E. Structural, magnetic, optical properties and cation distribution of nanosized $Co_{0.7}Zn_{0.3}Tm_xFe_{2-x}O_4$ (0.0 \leq x \leq 0.04) spinel ferrites synthesized by ultrasonic ultrasonic irradiation. Ultrason. Sonochem. 2019, 58, 104638. https://doi.org/10.1016/j .ultsonch.2019.104638.
- 16. Rathi P. L., Deepa S. Structural, magnetic, thermal and optical properties of Sn²⁺ cation doped magnetite nanoparticles. Ceram. Int. 2020, 46, 2969 – 2978. https://doi.org/10.1016/j.ceramint.2019 .09.294.
- 17. Heidari P., Masoudpanah S. M. Structural, magnetic and optical properties and photocatalytic activity of magnesium-calcium ferrite powders. J. Phys. Chem. Solid. 2021, 148, 109681. https://doi .org/10.1016/j.jpcs.2020.109681.
- 18. Amin N., Sajjad M., Hasan U., Majeed Z., Latif Z., Ajaz M., Mahmood K., Ali A., Mehmood K., Fatima M., Akhtar M., Imran M., Bibi A., Zahir M., Jabeen F., Bano N. Structural, electrical, optical and dielectric properties of yttrium substituted cadmium ferrites prepared by Co-Precipitation method. Ceram. Int. 2020, 46, 20798 - 20809. https://doi.org/10.1016/j.ceramint.2020.05.079.
- 19. Fe Z., Li Z., Fe O., Lal G., Punia K., Narain S., Alvi P. A., Choudhary B. L., Kumar S. J. Alloys Compd. 2020, 828, 1-6. https://doi.org/10 .1016/j.jallcom.2020.154388.
- 20. Slimani Y., Almessiere M. A., Sertkol M., Shirsath S. E., Baykal A., Nawaz M., Akhtar S., Ozcelik B., Ercan I. Structural, magnetic, optical properties and cation distribution of nanosized ultrasound irradiation. *Ultrason. Sonochem.* 2019, 57, 203 – 211. https://doi.org/ 10.1016/i.ultsonch.2019.05.001.
- 21. Gu D., Gu S. Magnetic properties, anticancer and antibacterial effectiveness of sonochemically produced. Arabian J. Chem. 2020, 7403 – 7417. https://doi.org/10.1016/j.arabjc.2020.08.017.
- 22. Almessiere M. A., Korkmaz A. D., Slimani Y., Nawaz M., Ali S., Baykal A. Magneto-optical properties of rare earth metals substituted Co-Zn spinel nanoferrites, *Ceram. Int.* 2019, 45, 3449-3458. https://doi.org/10.1016/j.ceramint.2018.10.260.
- 23. Dhiwahar A. T., Sundararajan M., Sakthivel P., Sekhar C., Yuvaraj S. Microwave-assisted combustion synthesis of pure and zinc-doped copper ferrite nanoparticles: structural, morphological, optical, vibrational, and magnetic behavior. J. Phys. Chem. Solid. 2020, 138, 109257. https://doi.org/10.1016/j.jpcs.2019.109257.
- 24. Hussain K., Bibi A., Jabeen F., Amin N., Mahmood K., Ali A., Iqbal M. Z., Arshad M. I. Study of structural, optical, electrical and magnetic properties of Cu_{2b} doped Zn_{0.4}Co_{0.6-x}Ce_{0.1}Fe_{1.9}O₄ spinel ferrites. Physica B: Phys. Condens. Matter 2020, 584, 412078. https://doi.org/ 10.1016/j.physb.2020.412078.
- 25. Sundararajan M., Kennedy L. J., Aruldoss U., Khadeer S., Vijaya J. J., Dunn S. Microwave combustion synthesis of zinc substituted nanocrystalline spinel cobalt ferrite: structural and magnetic studies. Mater. Sci. Semicond. Process. 2015, 40, 1-10. https://doi .org/10.1016/j.mssp.2015.06.002.
- 26. Lassoued A., Li J. F. Magnetic and photocatalytic properties of Ni Co ferrites. Solid State Sci. 2020, 104, 1-13. https://doi.org/10.1016/ i.solidstatesciences.2020.106199.

- 27. Chakrabarty S., Bandyopadhyay S., Pal M., Dutta A. Sol-gel derived cobalt containing Ni - Zn ferrite nanoparticles: dielectric relaxation and enhanced magnetic property study. Mater. Chem. Phys. 2021, 259, 124193. https://doi.org/10.1016/j.matchemphys .2020.124193.
- 28. Singh R., Ku I., Vilcakova J., Jamatia T., Machovsky M., Skoda D., Urbánek P., Masa M., Urbánek M., Kalina L., Havlica J. Impact of sonochemical synthesis condition on the structural and physical properties of MnFe₂O₄ spinel ferrite nanoparticles. *Ultrason*. Sonochem. 2020, 61, 1-15. https://doi.org/10.1016/j.ultsonch.2019 .104839.
- 29. Hammad T. M., Salem J. K., Abu A., Hejazy N. K. Optical and magnetic characterizations of zinc substituted copper ferrite synthesized by a co-precipitation chemical method. *I. Alloys Compd.* 2018, 741, 123-130. https://doi.org/10.1016/j.jallcom.2018.01.123.
- 30. Yousaf M., Niaz M., Wang B., Noor A. Preparations, optical, structural, conductive and magnetic evaluations of RE's (Pr, Y, Gd, Ho, Yb) doped spinel nanoferrites. Ceram. Int. 2020, 46, 4280 - 4288. https://doi.org/10.1016/j.ceramint.2019.10.149.
- 31. Dhiman M., Chudasama B., Kumar V., Tikoo K. B., Singhal S. Augmenting the photocatalytic performance of cobalt ferrite via change in structural and optical properties with the introduction of different rare earth metal ions. Ceram. Int. 2019, 45, 3698 – 3709. https://doi.org/10.1016/j.ceramint.2018.11.033.
- 32. Saini M., Shukla R., Kumar A. Cd²⁺ substituted nickel ferrite doped polyaniline nanocomposites as effective shield against electromagnetic radiation in X-band frequency. J. Magn. Magn. Mater. 2019, 491, 165549. https://doi.org/10.1016/j.jmmm.2019 .165549.
- 33. Rajeshwari A., Punithavthy I. K., Jeyakumar S. J., Lenin N., Vigneshwaran B. Dependance of lanthanum ions on structural, magnetic and electrical of manganese based spinel nanoferrites. Ceram. Int. 2020, 46, 6860 – 6870. https://doi.org/10.1016/j .ceramint.2019.11.180.
- 34. Tatarchuk T. R., Paliychuk N. D., Bououdina M., Al-najar B., Pacia M., Macyk W. Effect of cobalt substitution on structural, elastic, magnetic and optical properties of zinc ferrite nanoparticles. J. Alloys Compd. 2018, 731, 1256-1266. https://doi.org/10.1016/j .jallcom.2017.10.103.
- 35. Co M., Fe O., Verma V., Kaur M., Marc I. Tailored structural, optical and magnetic properties of ternary nanohybrid. Ceram. Int. 2019, 45, 10865 – 10875. https://doi.org/10.1016/j.ceramint.2019.02.164.
- 36. Andhare D. D., Patade S. R., Kounsalye J. S., Jadhav K. M. Effect of Zn doping on structural, magnetic and optical properties of cobalt ferrite nanoparticles synthesized via. Co-precipitation method. Physica B: Phys. Condens. Matter 2020, 583, 412051. https://doi.org/ 10.1016/j.physb.2020.412051.
- 37. Abraham A. G., Manikandan A., Manikandan E., Vadivel S., Jaganathan S. K., Baykal A., Renganathan P. S. Enhanced magneto-optical and photo-catalytic properties of transition metal cobalt (Co²⁺ ions) doped spinel MgFe₂O₄ ferrite nanocomposites. *J. Magn. Magn Mater.* 2018, 452, 380 – 388. https://doi.org/10.1016/j .immm.2018.01.001.
- 38. Hussain K., Amin N., Arshad M. I. Evaluation of structural, optical, dielectric, electrical, and magnetic properties of Ce³⁺ doped Cu_{0.5}Cd_{0.25}Co_{0.25}Fe_{2-x}O₄ spinel nano-ferrites. *Ceram. Int.* 2021, 47, 3401-3410. https://doi.org/10.1016/j.ceramint.2020.09.185.
- 39. Dhiwahar A. T., Maruthamuthu S., Marnadu R., Sundararajan M., Manthrammel M. A., Shkir M., Sakthivel P., Reddy V., Reddy M.

- Improved photocatalytic degradation of rhodamine B under visible light and magnetic properties using microwave combustion grown Ni doped copper ferrite spinel nanoparticles. Solid State Sci. 2021, 113, 106542. https://doi.org/10.1016/j.solidstatesciences.2021 .106542.
- 40. Vinosha P. A., Manikandan A., Ragu R., Dinesh A., Thanrasu K., Slimani Y., Baykal A., Xavier B. Impact of nickel substitution on structure, magneto-optical, electrical and acoustical properties of cobalt ferrite nanoparticles. J. Alloys Compd. 2021, 857, 157517. https://doi.org/10.1016/j.jallcom.2020.157517.
- 41. Naresh U., Kumar R. J., Babu K. C. Hydrothermal synthesis of barium copper ferrite nanoparticles: nanofiber formation, optical, and magnetic properties. Mater. Chem. Phys. 2019, 236, 121807. https://doi.org/10.1016/j.matchemphys.2019
- 42. Ateia E. E., Mohamed A. T., Elsayed K. Impact of Gd³⁺/graphene substitution on the physical properties of magnesium ferrite nanocomposites. J. Magn. Magn Mater. 2018, 452, 169—178. https:// doi.org/10.1016/j.jmmm.2017.12.053.
- 43. Sharma R., Thakur P., Sharma P., Sharma V. Ferrimagnetic Ni_{2b} doped Mg-Zn spinel ferrite nanoparticles for high density information storage. J. Alloys Compd. 2017, 704, 7-17. https://doi .org/10.1016/j.jallcom.2017.02.021.
- 44. Kardile H. J., Somvanshi S. B., Chavan A. R., Pandit A. A., Jadhav K. M. Effect of Cd²⁺ doping on structural, morphological, optical, magnetic and wettability properties of nickel ferrite thin films. Optik — Int. J. Light Electron Opt. 2020, 207, 164462. https://doi.org/ 10.1016/j.ijleo.2020.164462.
- 45. Yuvaraj S., Manikandan N., Vinitha G. Influence of copper ions on structural and non-linear optical properties in manganese ferrite nanomaterials. Opt. Mater. 2017, 73, 428-436. https://doi.org/10 .1016/j.optmat.2017.08.027.
- 46. Iftikhar S., Faroog M., Haider S., Musaddig S., Shakir I., Shahid M. The impact of carbon nanotubes on the optical, electrical, and magnetic parameters of Ni²⁺ and Co²⁺ based spinel ferrites. Ceram. Int. 2019, 45, 21150 - 21161. https://doi.org/10.1016/j .ceramint.2019.07.092.
- 47. Al-ghamdi A. A., Al-hazmi F. S., Memesh L. S., Shokr F. S., Bronstein M. Effect of mechanochemical synthesis on the structure, magnetic and optical behavior of Ni_{1-x}Zn_xFe₂O₄ spinel ferrites. Ceram. Int. 2017, 43, 6192-6200. https://doi.org/10.1016/j.ceramint .2017.02.017.
- 48. Iranmanesh P., Tabatabai S., Mehran M. Effect of Ni substitution on structural, optical and magnetic properties of ferrite nanoparticles synthesized by co-precipitation route. Mater. Sci. Eng. B 2019, 251, 114442. https://doi.org/10.1016/j.mseb.2019.114442.
- 49. Mohsin M., Ansari N., Khan S., Ahmad N. Effect of R³⁺ (R = Pr, Nd, Eu and Gd) substitution on the structural, electrical, magnetic and optical properties of Mn-ferrite nanoparticles. J. Magn. Magn Mater. 2018, 465, 81-87. https://doi.org/10.1016/j.jmmm.2018.05
- 50. Patil S., Anantharaju K. S., Rangappa D., Vidya Y. S., Sharma S. C., Renuka L., Nagabhushana H. Magnetic Eu-doped MgFe₂O₄ nanomaterials: an investigation of their structural, optical and enhanced visible-light-driven photocatalytic performance. Environ. Nanotechnol. Monit. Manag. 2020, 13, 100268. https://doi.org/10 .1016/j.enmm.2019.100268.
- 51. Ur A., Morley N. A., Amin N., Imran M., Ajaz M., Mahmood K., Ali A., Aslam A., Bibi A., Zahir M., Igbal F., Bano N., Alzaid M. Controllable

- synthesis of La^{3+} doped $Zn_{0.5}Co_{0.25}Cu_{0.25}Fe_{2-x}La_xO_4$ (x = 0.0, 0.0125, 0.025, 0.0375, 0.05) nano-ferrites by sol-gel auto-combustion route. Ceram. Int. 2020, 46, 29297 – 29308. https://doi.org/10.1016/j.ceramint.2020.08.106.
- 52. Dojcinovic M. P., Vasiljevic Z. Z., Pavlovic V. P., Barisic D., Pajic D., Tadic N. B., Vesna M. Mixed MgeCo spinel ferrites: structure, morphology, magnetic and photocatalytic properties. J. Alloys Compd. 2021, 855, 157429. https://doi.org/10.1016/j.jallcom.2020 .157429.
- 53. Zeeshan T., Waseem S., Riaz M., Zia R. Ceram. Int. 2020, 46, 3935 - 3943. https://doi.org/10.1016/j.ceramint.2019.10.122.
- 54. Ashok A., Kennedy L. J., Vijaya J. J. Structural, optical and magnetic properties of Zn_{1-x}Mn_xFe₂O₄ (0 x 0.5) spinel nano particles for transesteri fi cation of used cooking oil. *J. Alloys Compd.* 2019, 780, 816-828. https://doi.org/10.1016/j.jallcom.2018.11.390.
- 55. Shokri A., Farjami S., Boustani K. The role of Co ion substitution in SnFe₂O₄ spinel ferrite nanoparticles: study of structural, vibrational, magnetic and optical properties. Ceram. Int. 2018, 44, 22092-22101. https://doi.org/10.1016/j.ceramint.2018.08.319.

- 56. Kumar N., Kr R., Kumar S., Kumar P. Tuning in optical, magnetic and Curie temperature behaviour of nickel ferrite by substitution of monovalent K^{+1} ion of $Ni_{0.8}K_{0.2}Fe_2O_4$ nanomaterials for multifunctional applications. Physica B: Phys. Condens. Matter 2021, 606, 412797. https://doi.org/10.1016/j.physb.2020.412797.
- 57. Sundararajan M., Kennedy L. J., Nithya P., Vijaya J. J., Bououdina M. Visible light driven photocatalytic degradation of rhodamine B using Mg doped cobalt ferrite spinel nanoparticles synthesized by microwave combustion method. J. Phys. Chem. Solids 2017, 108, 61-75. https://doi.org/10.1016/j.jpcs.2017.04.002.
- 58. Lassoued A., Lassoued M. S., Dkhil B., Ammar S., Gadri A. Substituted effect of Al³⁺ on structural, optical, magnetic and photocatalytic activity of Ni ferrites. J. Magn. Magn Mater. 2019, 476, 124-133. https://doi.org/10.1016/j.jmmm.2018.12.062.
- 59. Somvanshi S. B., Jadhav S. A., Khedkar M. V., Kharat P. B., More S. D., Jadhav K. M. Structural, thermal, spectral, optical and surface analysis of rare earth metal ion (Gd^{3+}) doped mixed Zn - Mgnano-spinel ferrites. Ceram. Int. 2020, 46, 13170 – 13179. https://doi .org/10.1016/j.ceramint.2020.02.091.